Non-Terrestrial Networks: Link Budget Analysis

Alessandro Guidotti*, *Member, IEEE* Alessandro Vanelli-Coralli*, *Senior Member, IEEE*,
Alberto Mengali†, Stefano Cioni†, *Member, IEEE*
*Department of Electrical, Electronic, and Information Engineering (DEI) "Guglielmo Marconi," Univ. of Bologna, Italy
†European Space Agency - esa.int, ESTEC/TEC-EST, Noordwijk, The Netherlands.

***Abstract*—Satellite Communication systems represent a solid solution to extend and complement terrestrial networks in un-/under-served areas. The recent standardisation endeavours within 3GPP led to the Non-Terrestrial Networks (NTN) study item for New Radio, aimed at deploying satellite systems either stand-alone or as integration to terrestrial networks in mobile broadband and machine-type communication scenarios. In this context, the main focus is currently related to: i) evaluating the system level performance; and ii) understanding the impact at link level of typical satellite channel impairments on the PHY/MAC procedures. In this paper, we focus on the former; in particular, we provide: i) a detailed discussion on the current system architecture and assumptions; ii) we thoroughly describe the methodology to perform link budget computations; and iii) we show the numerical results for GEO and LEO systems.**

***Index Terms*—Satellite Communications, 5G, New Radio, Non-Terrestrial Networks, Link Budget.**

I. Introduction

During the last years, the evolution of future communication networks has been not only aiming at larger throughputs, but also at providing a set of extremely diverse services characterised by significantly different requirements in terms of latency, security, and reliability. The vision provided by ITU for future systems back in 2015 highlighted a set of technical requirements, which come along with other key drivers as the emergence of Internet of things (IoT), *i.e.*, billions of objects connected to the Internet, which is the enabler for smart cities, or the need to ensure network reliability, robustness, and availability, as well as cybersecurity, [1]. In this context, terrestrial systems are coping with these challenges by means of the definition of a novel communication standard, dubbed as 5G or, in 3GPP nomenclature, New Radio (NR), [2]–[4]. The massive scientific and industrial interest in NR systems is motivated by the pivotal role that these systems will play in the worldwide economic and societal processes to support the next generation of vertical services, [5], [6]. The first standard for NR systems has been released at the end of 2018, as reference for enhanced Mobile Broadband (eMBB) communications below 6 GHz; NR networks are now being deployed, with many 5G field trials on-going for testing more advanced technologies expected for future releases, [7], [8]. Future 3GPP releases will include ultra-Reliable and Low-Latency Communications (URLLC) and massive Machine-Type Communications (mMTC) systems also above 6 GHz.

In the above landscape, the integration of satellite and terrestrial networks can be a cornerstone to the realisation of the foreseen heterogeneous global system to enhance the end user experience. Due to their inherently large footprint, satellites can efficiently complement and extend dense terrestrial networks, both in densely populated areas and in rural zones, as well as provide reliable Mission Critical services. In the past, there has been a loose interaction between the satellite and terrestrial communities, which have developed almost independently from each other, and this led to a difficult *a posteriori* integration between the two systems to provide seamless services. For instance, in [9]–[13], interesting insights are provided on the integration, and related difficulties, of Long Term Evolution (LTE) systems in SatCom. Thanks to the initiation of the new 5G communication standards, and learning from past experience, the satellite and terrestrial communities are now working together to realise a fully fledged satellite-terrestrial architecture based on the 5G ecosystem. This is reflected, within 3GPP, by a recent Study Item on Non-Terrestrial Networks (NTN), [14]–[16]. NTN systems are expected to support 5G services in isolated or remote areas that are un-/under-served by terrestrial networks, to reinforce the 5G service reliability and continuity for M2M and IoT, and to enable 5G network scalability. The integration of satellite and terrestrial networks, and in particular the impact that satellite typical impairments might have on the 5G air interface and protocols, poses the need to address key aspects related to physical layer (PHY), as well as possible modifications to the upper layer procedures. These aspects have been addressed in several scientific papers, [17]–[20], and projects, [21], [22]. In [17]–[19], the authors focus was on PHY/MAC layer techniques that shall cope with typical satellite channel impairments; in particular, the first PHY standard has been made available and preliminary analyses related to the deployment of 5G systems through SatCom are advancing. Finally, in [20], a detailed analysis on the impact of PHY/MAC timing constraints on the beam size is provided.

In this paper, we focus on the preliminary performance assessment of 3GPP NTN systems. In particular, we provide a detailed overview of the NTN system architectures currently considered within 3GPP and then discuss on the system layout and assumptions to perform the link budget calibration in both

This work has been supported by European Space Agency (ESA) ARTES Advanced Technology (3C.017) project "Spin-In of 3GPP terrestrial radio access technology for SATCOM." Opinions, interpretations, recommendations and conclusions presented in this paper are those of the authors and are not necessarily endorsed by the European Space Agency.

978-1-7281-5089-5/20/$31.00 ©2020 IEEE

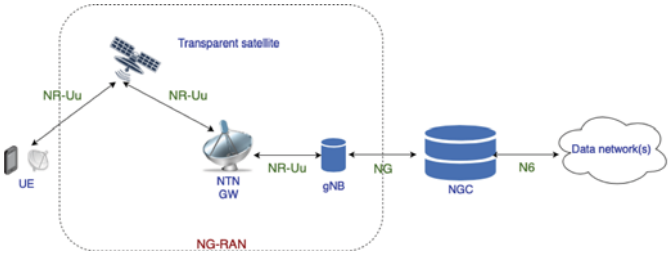

Fig. 1. High-level system architecture: transparent payload and direct access.

the downlink and the uplink. These aspects are currently the main point being addressed within 3GPP RAN meetings, since they will provide key information for the NTN consolidation.

II. System Architecture and Geometry

A. Architecture

The high-level system architecture is shown in Figure 1. The following network elements can be identified, [15]: i) a User Equipment (UE), which can be fixed or mobile; ii) a transparent payload satellite or Unmanned Aircraft System (UAS), providing NR connectivity to the UE through the user access link; iii) a system gateway (GW) interconnecting the flying platform (satellite/UAS) with the NR infrastructure; and iv) a NR gNB conceptually located at the GW, providing connectivity towards the Next Generation Core network (NGC). It is worthwhile highlighting that any communication between the UE and the corresponding gNB is performed by means of the standardised NR-Uu air interface, [3], [4]; thus, the gNB-GW, GW-satellite/UAS, and satellite/UAS-UE links are all based on the NR-Uu air interface. This reference architecture can be declined into different scenarios, depending on the orbit and altitude of the flying platform, as reported in Table I. When Low Earth Orbit (LEO) platforms are considered, the on-ground beams can be either fixed, *i.e.*, the on-board antenna keeps serving the same on-ground beam while the satellite moves on its orbit (steerable antennas), or moving, *i.e.*, the served on-ground beam is moving together with the satellite.

The above depicted NTN system architecture is characterised by *direct access* to the UEs and a *transparent payload* on-board the flying platform. However, it shall be noticed that NTN systems can also be based on regenerative payloads, which would allow to implement gNB functionalities on-board the satellite and, thus, more advanced system configurations, such as functional split and inter-satellite links (ISLs), [15]. In this paper, if not otherwise specified, we assume the following system configuration: i) direct access; ii) transparent payload; iii) a single LEO or GEO multi-beam platform operating in Ka-band; and iv) moving beams for LEO constellations. These assumptions are those currently addressed in the NTN standardisation for preliminary system level analyses. As for the UEs, Very Small Aperture Terminal (VSAT) terminals are considered; however, it is worth highlighting that handheld terminals are foreseen for S-band systems and UEs for moving platforms are currently being discussed within 3GPP.

TABLE I
NTN orbits and altitudes, [15].

Platform	Altitude	Orbit
Low Earth Orbit (LEO)	$300 - 1500$ km	circular
Medium Earth Orbit (MEO)	$7000 - 25000$ km	circular
Geostationary Earth Orbit (GEO)	35786 km	fixed
UAS	$8 - 50$ km	fixed
Elliptical Earth Orbit (HEO)	$400 - 50000$ km	elliptical

B. Geometry

In order to define the multi-beam layout on the considered service area, we consider the system geometry shown in Figure 2, in which (x_E, y_E, z_E) denote the Earth-Centred Earth-Fixed (ECEF) coordinates. For a given transmitting antenna configuration (and, thus, radiation pattern), the 3 dB angle ϑ_{3dB} is defined as the angle with respect to the antenna boresight direction at which the radiation pattern is equal to -3 dB. Once ϑ_{3dB} is known, the beam radius, R_{3dB}, is defined as the radius of a circular beam centred at the Sub Satellite Point (SSP) having its edge at ϑ_{3dB}. Then, the following two steps are performed to define the beam centre locations: i) implement a hexagonal tessellation based on the obtained beam radius on a plane; and ii) project the beam centres locations on the curve surface of the Earth.

As for the hexagonal tessellation, let us consider a plane tangent to the Earth's surface at the SSP and a generic point P on it. Let us also assume that the considered system geometry is normalised so as to have a satellite with unit altitude, *i.e.*, distances are normalised to h_{sat} and coordinates to $\sqrt{h_{sat}}$. In this system, we introduce the (u, v) coordinates centred in the SSP with: i) the v unit vector being oriented as the ECEF z_E-axis; and ii) the u unit vector being parallel to the ECEF y_E-axis and oriented in the opposite direction. These two unit vectors are the direction cosines corresponding to the ϑ and ϕ look angles from the satellite, [15], [23]:

$$\begin{aligned} u &= \sin\vartheta\cos\phi \\ v &= \sin\vartheta\sin\phi \end{aligned} \tag{1}$$

where, from the satellite perspective, ϑ is the angle between the direction of P and that of the SSP and ϕ is the clockwise angle between P and the v-axis. For $\vartheta = \vartheta_{3dB}$, we obtain the beam radius in the uv coordinate system:

$$R_{3dB}^{(uv)} = \sqrt{u_P^2 + v_P^2} = \sin\vartheta_{3dB} \tag{2}$$

where we exploited the conversion formulae in eq. (1). The hexagonal tessellation on the uv plane is obtained by locating the adjacent beam centres at the following distance:

$$ABS = 2R_{3dB}^{(uv)}\frac{\sqrt{3}}{2} = R_{3dB}^{(uv)}\sqrt{3} \overset{(a)}{=} \sqrt{3}\sin\vartheta_{3dB} \tag{3}$$

where in (a) we exploited eq. (2). Once the hexagonal tessellation has been performed on the uv plane, each location is projected to the Earth's surface by: i) removing the normalisation, *i.e.*, multiplying the coordinates by $\sqrt{h_{sat}}$, to obtain the coordinates on the plane in (x_E, y_E, z_E); and ii)

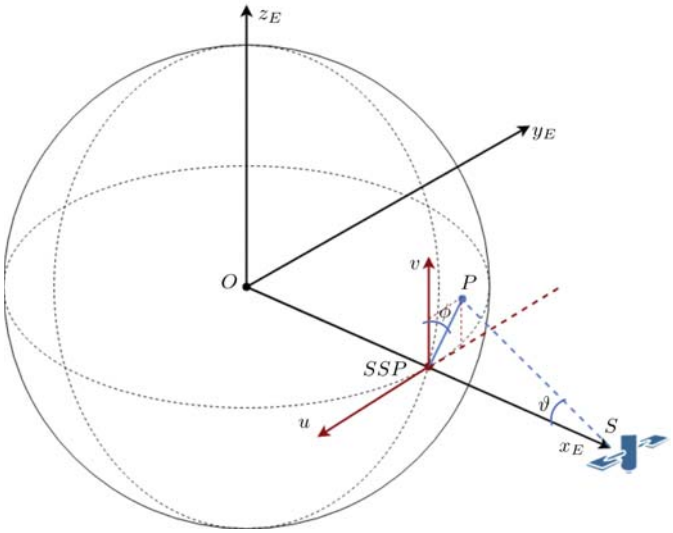

Fig. 2. System geometry for the beam layout definition.

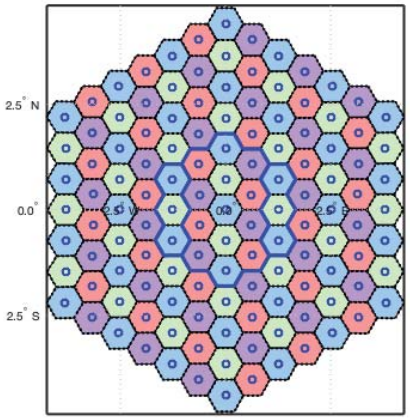

Fig. 3. Example of beam layout in (LAT, LON). Setup: LEO system in Ka-band at $h_{sat} = 1200$ km, frequency reuse 4, 127 beams. The thick blue line denotes the beams retained for performance evaluation.

compute the intersection between the Earth's surface and the line passing through the beam centre location and the satellite. These coordinates can then be easily converted to latitude and longitude (LAT, LON).

Three different frequency reuse schemes are considered, [15]: i) full frequency reuse (FFR); ii) frequency reuse 3 (FR3), with the available bandwidth split into 3 orthogonal channels; and iii) frequency reuse 4 (FR4), in which the bandwidth is split into two channels and two orthogonal polarisations.

In [15], the values of ABS for LEO and GEO systems, both in Ka- and S- bands, are provided assuming the following Bessel radiation pattern for the satellite antennas, [16]:

$$\Omega(\vartheta) = \begin{cases} 1, & \vartheta = 0 \\ 4\left|\frac{J_1(ka\sin\vartheta)}{ka\sin\vartheta}\right|^2, & \vartheta \neq 0 \end{cases} \quad (4)$$

where: i) a is the antenna aperture radius; ii) $k = 2\pi f_c/c$ is the wave number, with f_c being the operating frequency and c the speed of light; iii) $J_1(\cdot)$ is the Bessel function of the first order; and iv) ϑ is the angle measured from the boresight of the antenna's main beam. Since in this work we focus on Ka-band systems, both the UE and satellite antennas are modelled as in (4) as per 3GPP specifications in [15].

III. Link Budget Computation

In this Section, we discuss the methodology to obtain the downlink and uplink link budget for the considered system.

A. Path losses

The overall path loss is defined as, [15], [16]:

$$PL = PL_b + PL_{atm} + PL_s \quad (5)$$

where: i) PL_b is the basic path loss, which combines free space, clutter, and shadowing losses; ii) PL_{atm} represents the losses due to atmospheric gases; and iii) PL_s represents the signal loss due to tropospheric or ionospheric scintillations.

a) Basic path loss: : this term is the combination of free space loss PL_{fs}, clutter loss PL_{cl}, and lognormal shadowing PL_σ:

$$PL_b = PL_{fs} + PL_\sigma + PL_{cl} \overset{(a)}{=} PL_{fs} + PL_\sigma \quad (6)$$

where in (a) it is assumed that the user is always in Line of Sight (LoS) conditions and, thus, PL_{cl} is always null, [15]. For a generic user located at slant range d from the satellite, the free space loss is given by:

$$PL_{fs} = 32.45 + 20\log_{10} f_c[\text{GHz}] + 20\log_{10} d[\text{m}] \quad (7)$$

where f_c is the operating frequency. As for the lognormal shadowing, PL_σ is modelled as a lognormal random variable with zero mean and a variance related to the harshness of the shadowing environment, *i.e.*, $PL_\sigma \sim (0, \sigma_s^2)$. The values of σ_s^2 are provided by 3GPP for dense urban, urban, and rural scenarios as a function of the elevation angle, [16].

b) Atmospheric losses: the term PL_{atm} taking into account the atmospheric losses is computed as provided in Annex 2 of ITU-R P.676 for slant paths. The atmosphere is modelled with temperature 288.15 K, pressure 1013.25 hPa, and water vapour density 7.5 g/m^3.

c) Scintillation: the tropospheric scintillations, impacting signals in Ka-band, are modelled as a fixed term depending on the user elevation angle, [16]. These values are obtained by means of the procedure described in ITU-R P.618, [25]. Ionospheric scintillations are not considered in Ka-band.

B. Downlink

For the downlink computation, the reference scheme is shown in Figure 4, where: i) the intended u-th user is randomly located inside the intended b-th beam; ii) an interfering signal is transmitted from the i-th antenna towards the j-th user of the i-th beam; iii) $d_{b,u}$ is the slant range of the u-th user in

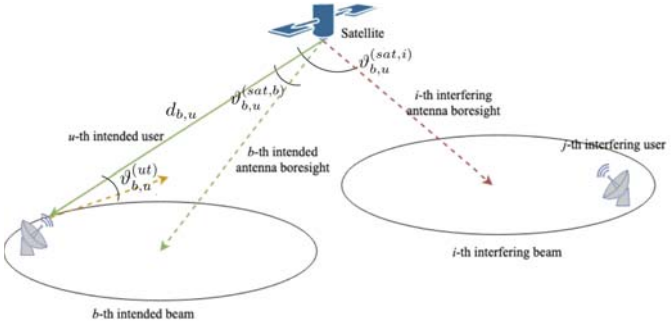

Fig. 4. Downlink geometry for link budget computation.

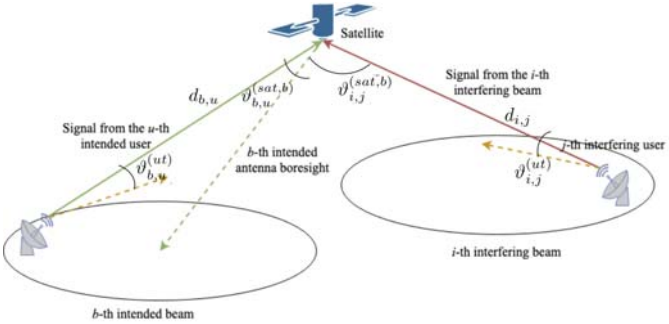

Fig. 5. Uplink geometry for link budget computation.

the b-th beam; iv) $\vartheta_{b,u}^{(sat,i)}$ denotes the angle between the i-th antenna boresight and the direction of the u-th user in the b-th beam (when $i = b$, this is the angle from the intended antenna boresight); and v) $\vartheta_{b,u}^{(ut)}$ denotes the angle between the antenna pointing of the u-th user in the b-th beam and the satellite, which does not depend on the satellite antenna index since they are assumed to be colocated. The intended power received by the u-th user in the b-th beam is given by:

$$C_{b,u}^{(DL)} = EIRP_{b,u}^{(DL)}\left(\vartheta_{b,u}^{(sat,b)}\right) + G_{RX}^{(ut)}\left(\vartheta_{b,u}^{(ut)}\right) - PL_{(b,u)}^{(DL)} \tag{8}$$

where: i) $G_{RX}^{(ut)}\left(\vartheta_{b,u}^{(ut)}\right)$ is the receiving antenna gain as a function of the angle between the UE antenna pointing and the satellite direction obtained from (4); ii) $EIRP_{b,u}^{(DL)}$ is the transmitted Equivalent Isotropically Radiated Power from the intended b-th antenna towards the u-th user; and iii) $PL_{(b,u)}^{(DL)}$ is the path loss for the u-th intended user in the b-th beam computed as in eq. (5). The transmitted EIRP is computed as:

$$EIRP_{b,u}^{(DL)}\left(\vartheta_{b,u}^{(sat,b)}\right) = EIRP_{max}^{(DL)} + 10\log_{10}\Omega\left(\vartheta_{b,u}^{(sat,b)}\right) \tag{9}$$

where $EIRP_{max}^{(DL)} = \delta_{EIRP} + 10\log_{10}\left(\frac{B}{r}\right)$ is the maximum EIRP, *i.e.*, the EIRP in the antenna boresight direction, with δ_{EIRP} being the EIRP density, B the overall bandwidth, and r a factor taking into account the bandwidth splitting due to frequency reuse: $r = 1$ for FFR, $r = 3$ for FR3, and $r = 2$ for FR4 (since it uses two channels and two polarisations). In the above formula, the radiation pattern of the satellite antenna is defined in eq. (4).

The noise power at the receiver is independent of the UE, *i.e.*, it is the same $\forall u, b$, and it can be computed as follows:

$$\begin{aligned} N^{(DL)} = N_f + 10\log_{10}\left(T_0 + (T_a - T_0)\,10^{-0.1N_f}\right) \\ + \kappa[\text{dBW/K/Hz}] + 10\log_{10}\left(\frac{B}{r}\right) \end{aligned} \tag{10}$$

where N_f is the receiver noise figure, T_a is the receiver antenna temperature, κ is the Boltzmann constant, and $T_0 = 290$ K is the reference noise temperature. The Carrier-to-Noise Ratio (CNR) is then obtained by subtracting (10) from (8).

Finally, the overall interference at the u-th user in the b-th beam is given by:

$$I_{b,u}^{(DL)} = 10\log_{10}\left(\sum_{j=1}^{N_{int}} 10^{0.1I_{b,u,i}^{(DL)}}\right) \tag{11}$$

where

$$I_{b,u,i}^{(DL)} = EIRP_{b,u}^{(DL)}\left(\vartheta_{b,u}^{(sat,i)}\right) + G_{RX}^{(ut)}\left(\vartheta_{b,u}^{(ut)}\right) - PL_{(b,u)}^{(DL)} \tag{12}$$

is the interference from the i-th interfering beam, with $i = 1, \ldots, N_{int}$ and N_{int} being the number of co-channel beams. It shall be noticed that, in the i-th interference term, the satellite EIRP is now computed based on the angle between the i-th interfering antenna boresight and the direction of the u-th intended user in the b-th beam. From eq. (11), it is straightforward to obtain the Carrier-to-Interference Ratio (CIR), $CIR_{b,u}^{(DL)}$, by subtracting (11) from eq. (8); the overall Carrier-to-Interference plus Noise Ratio (CINR) is given by:

$$CINR_{b,u}^{(DL)} = -10\log_{10}\left(10^{-0.1CNR_{b,u}^{(DL)}} + 10^{-0.1CIR_{b,u}^{(DL)}}\right) \tag{13}$$

It is worthwhile highlighting that the above formulation for the downlink performance can be applied to any of the systems foreseen for NTN in Table I.

C. Uplink

For the uplink, the reference scenario is depicted in Figure 5, where, in addition to the nomenclature introduced for the downlink, we have that: i) the interfering j-th user is randomly located inside the interfering i-th beam; ii) $d_{i,j}$ is the slant range of the j-th user in the i-th beam; iii) $\vartheta_{i,j}^{(sat,b)}$ denotes the angle between the receiving b-th antenna boresight and the direction of arrival of the interfering signal from the j-th user in the i-th beam; and iv) $\vartheta_{i,j}^{(ut)}$ denotes the angle between the antenna pointing of the j-th user in the i-th beam and the satellite, which does not depend on the satellite antenna index due to antenna colocation. The intended power received by the b-th satellite antenna from the u-th user is given by:

$$C_{b,u}^{(UL)} = EIRP_{b,u}^{(UL)}\left(\vartheta_{b,u}^{(ut)}\right) + G_{RX}^{(sat)}\left(\vartheta_{b,u}^{(sat,b)}\right) - PL_{(b,u)}^{(UL)} \tag{14}$$

TABLE II
SATELLITE PARAMETERS FOR KA-BAND LINK BUDGET EVALUATION, [15].

Parameter	GEO	LEO	
		Ka	
		600 km	1200 km
Equivalent antenna radius a [m]	2.5	0.25	0.25
EIRP density δ_{EIRP} [dBW/MHz]	40	4	10
max. TX gain $G_{TX,max}^{(sat)}$ [dBi]	58.5	38.5	38.5
max. RX gain $G_{RX,max}^{(sat)}$ [dBi]	62	42	42
G/T [dB/K]	28	13	13

TABLE III
VSAT PARAMETERS FOR THE LINK BUDGET EVALUATION, [15].

Parameter	Value
Polarisation	circular
max. TX gain $G_{TX,max}^{(ut)}$ [dBi]	43.2
max. RX gain $G_{RX,max}^{(ut)}$ [dBi]	39.7
Transmission power $P_{TX}^{(ut)}$ [dBm]	33
Antenna temperature T_a [K]	150
Noise figure N_f [dB]	1.2

where, differently from the downlink: i) the EIRP is a function of the UE antenna radiation pattern; and ii) the receiving antenna gain is a function of that of the satellite:

$$EIRP_{b,u}^{(UL)}\left(\vartheta_{b,u}^{(ut)}\right) = EIRP_{max}^{(UL)} + 10\log_{10}\Omega\left(\vartheta_{b,u}^{(ut)}\right) \quad (15)$$

with $EIRP_{max}^{(UL)} = P_{TX}^{(ut)} + G_{TX,max}^{(ut)}$, in which $P_{TX}^{(ut)}$ is the transmission power of the considered UT type. The noise power in the uplink is computed as follows:

$$N^{(UL)} = 10\log_{10}\left(\kappa T\frac{B}{r}\right) \quad (16)$$

where T is the satellite antenna equivalent noise temperature. The uplink CNR, $CNR_{b,u}^{(UL)}$ is thus obtained by subtracting (16) from (14). The overall interference in the uplink, $I_{b,u}^{(UL)}$, can be easily obtained from the downlink case in eq. (11), with

$$I_{b,u,i}^{(UL)} = EIRP_{i,j}^{(UL)}\left(\vartheta_{i,j}^{(ut)}\right) + G_{RX}^{(sat)}\left(\vartheta_{i,j}^{(sat,b)}\right) - PL_{(i,j)}^{(UL)} \quad (17)$$

being the interference from the j-th user in the i-th beam. As in the downlink scenario, the CIR, $CIR_{b,u}^{(UL)}$, is obtained by subtracting (17) from (14) and the CINR, $CINR_{b,u}^{(UL)}$, is obtained as in eq. (13).

IV. NUMERICAL RESULTS

The link budget analysis is performed by means of Monte Carlo simulations based on the configuration reported in Tables from II to IV. In particular: i) the satellite is assumed to be on the equatorial plane at longitude $\ell_{sat} = 0°$; ii) the beams are located so as to have the satellite at $45°$ (GEO) or at $90°$ (LEO) elevation from the coverage center; and iii) the UEs' antennas are ideally pointed in the satellite direction, *i.e.*, the UE transmission or reception gain is always maximum. Finally, it shall be noticed that the methodology and assumptions are based on the agreements in 3GPP RAN meetings up to September 2019, [15].

TABLE IV
PARAMETERS FOR THE NUMERICAL EVALUATION, [15].

Parameter	Value
DL frequency	20 [GHz]
UL frequency	30 [GHz]
bandwidth	400 [MHz]
N. beams with FFR	61
N. beams with FR 3, 4	127
N. retained beams	19
Monte Carlo it.	100
Propagation	LOS, clear-sky

A variable number of tiers is considered depending on the frequency reuse scheme so as to ensure that the same number of interfering beams is considered for all scenarios; in order to properly model the overall interference experienced by each UE, the numerical results are gathered from the $N_B^{(sim)} = 19$ internal beams only, which are highlighted by the thick blue line in Figure 3 for the FR3 LEO case at 1200 km. With respect to the UEs, they are located on a (LAT, LON) grid over the whole coverage area, with resolution $0.05°$ for GEO, $0.02°$ for LEO at 1200 km, and $0.01°$ for LEO at 600 km.

It shall then be noticed that, in the DL, the interference towards any UE is generated by the co-channel transmitting antennas on the satellite; thus, interference is defined by geometry, *i.e.*, it is fixed given the receiving UE location and the beam layout configuration. Thus, the only stochastic aspect to be taken into account by means of Monte Carlo simulations is the shadow fading, modelled as a lognormal random variable $PL_\sigma \sim (0, \sigma_s^2)$, with the values of σ_s^2 depending on the UE's elevation angle, [16]. As for the uplink, interference is clearly depending on the specific interfering UEs locations, as highlighted by the presence of the terms $\vartheta_{i,j}^{(sat,b)}$ in eq. (17). Thus, in this case, Monte Carlo simulations deal with both the stochastic shadow fading and the interference source location; moreover, the latter is impacted by the scheduling algorithm, which, in the following, is assumed to be random.

Figures from 6 to 8 show the CIR and CINR Cumulative Distribution Functions (CDFs) for the downlink, while those from 9 to 11 for the uplink. Table V provides the mean and standard deviation of the CINR for all cases. In general, the CINR with FFR is quite low: the mean is between -1.49 dB (GEO UL) and -0.88 dB (LEO at 600 km UL) with a standard deviation in the order of $1.2-3.3$ dB for all scenarios; this is related to the severe interfering environment since no interference management technique, *e.g.*, precoding, is implemented for link budget calibration. Moving to FR3 or FR4 provides a significant performance improvement; focusing on GEO systems, the mean CINR is in the order of $7-8$ dB, with a 0.9 dB deviation in the DL, while in the UL these values are in the order of 2.7 dB, respectively. As for LEO systems, in the DL the mean CINR is similar to the GEO case, while in the UL it is in the order of $8.2-9.2$ dB; moreover, a significantly lower standard deviation is obtained with respect to GEO systems,

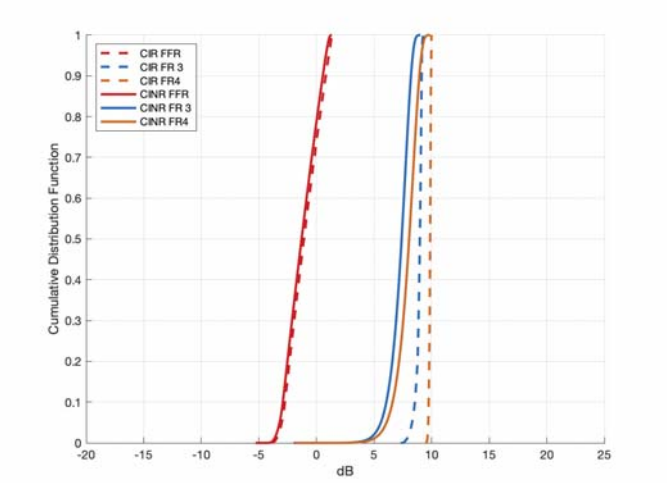

Fig. 6. Downlink link budget for GEO systems.

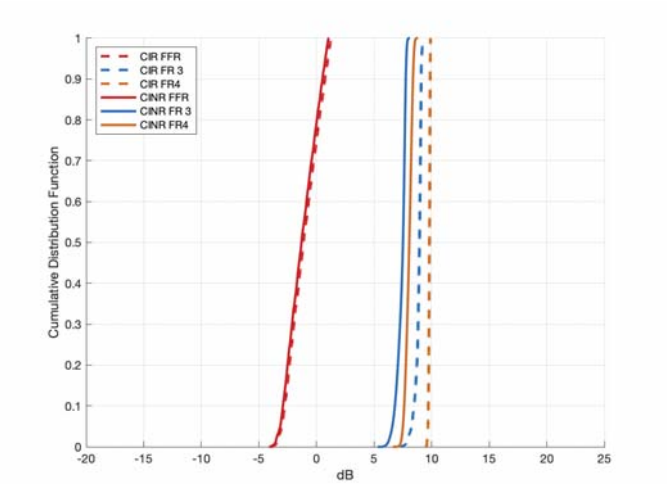

Fig. 7. Downlink link budget for LEO systems at 600 km.

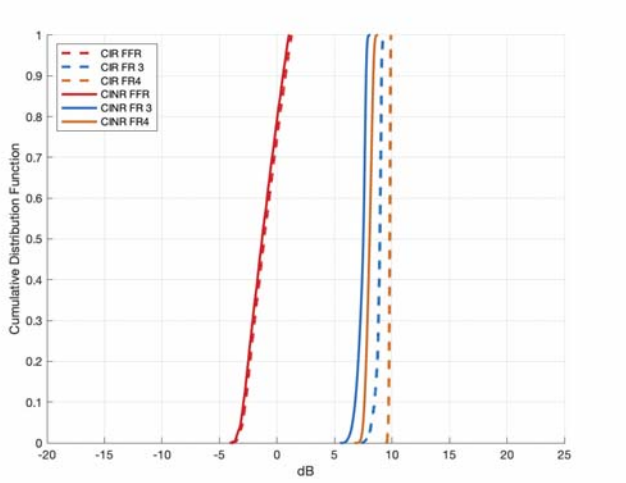

Fig. 8. Downlink link budget for LEO systems at 1200 km.

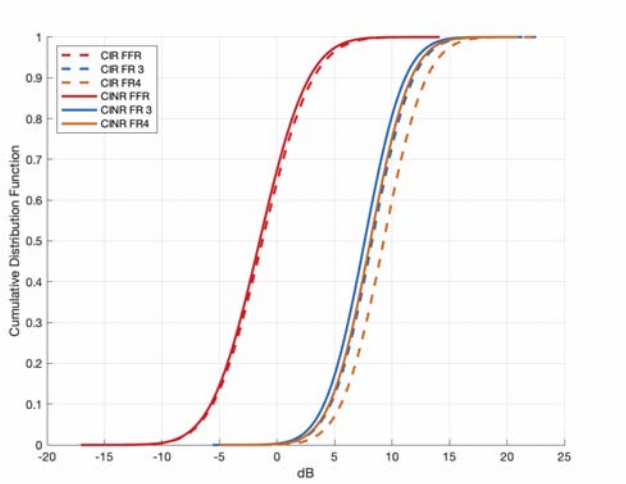

Fig. 9. Uplink link budget for GEO systems.

i.e., approximately half of the GEO case. This aspect is related to the significantly smaller coverage area when LEO systems are considered, which brings to more limited fluctuations when taking into account shadowing (related to the elevation angle) and slant range values. The significant difference in the standard deviation between the DL and the UL is motivated by the fact that, in the DL, interference is defined by geometry: the beam layout is fixed and the interfering satellite antennas are always transmitting towards their beam centers; in the UL, a random scheduling algorithm is implemented to identify the interfering users at each time frame and, thus, an increased variability arises. In general, as expected, unless interference management techniques like precoding are implemented, FFR schemes do not provide an efficient system, since most of the users would be in outage. The implementation of precoding is foreseen in NR systems by means of MMSE-IRC (Minimum Mean Square Error - Interference Rejection Combining), as reported in [27]. On the other hand, solutions with FR3 or FR4 already provide a good performance in terms of link budget; further system and link level analyses are currently being performed within 3GPP.

TABLE V
CINR MEAN, μ, AND STANDARD DEVIATION, σ IN DB.

Case		GEO		LEO600		LEO1200	
		μ	σ	μ	σ	μ	σ
DL	FFR	-1.25	1.28	-1.25	1.25	-1.25	1.25
	FR3	7.24	0.87	7.38	0.39	7.37	0.39
	FR4	7.88	0.95	8.03	0.29	8.02	0.29
UL	FFR	-1.49	3.34	-0.88	1.99	-0.96	1.98
	FR3	7.62	2.76	8.29	1.29	8.18	1.36
	FR4	8.12	2.79	9.25	1.45	9.16	1.48

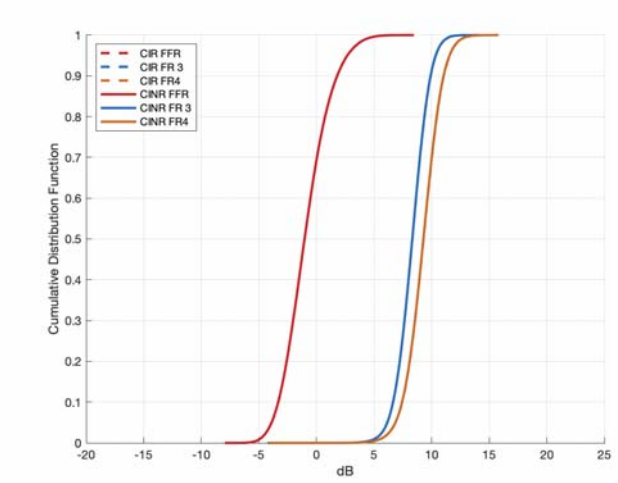

Fig. 10. Uplink link budget for LEO systems at 600 km.

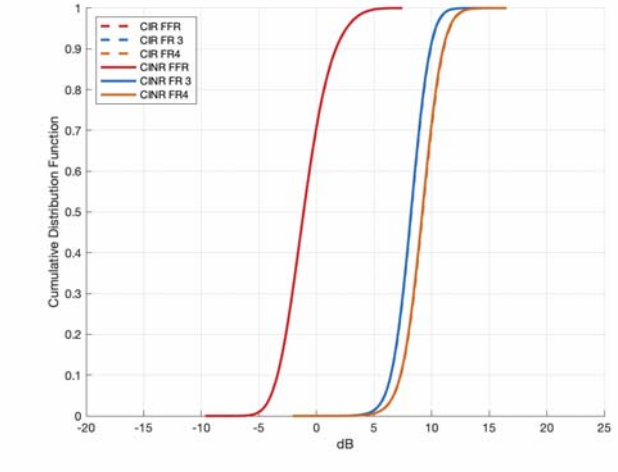

Fig. 11. Uplink link budget for LEO systems at 1200 km.

V. Conclusions

In this paper, we focused on the link budget calibration for GEO/LEO New Radio NTN systems in Ka-band. A detailed discussion on the current system architecture and assumptions was provided, together with a thorough description of the methodology. Numerical results were reported and discussed showing that FFR schemes require the implementation of interference management techniques, as MMSE-IRC, while for multi-colour FR schemes the link budget already provides a good performance. Finally, it is worthwhile highlighting that the NTN study item is on-going within 3GPP, which might lead to slightly different parameters for the performance assessment, or to additional scenarios as the implementation of handheld terminals, steerable antennas, or S-band systems.

References

[1] ITU-R M.2320-0, "Future technology trends of terrestrial IMT systems," November 2014.

[2] 3GPP TR 38.913, "Study on Scenarios and Requirements for Next Generation Access Technologies; (Release 14)," Jun. 2017.

[3] 3GPP TR 38.801, "Study on new radio access technology: Radio access architecture and interfaces (Release 14)," March 2017.

[4] 3GPP TR 38.211, "NR; Physical channels and modulation (Release 15)," March 2019.

[5] 5GPPP, 5G Empowering Vertical Industries, Feb. 2016. Available at: https://5g-ppp.eu/roadmaps/

[6] 5GPPP, 5G Innovations for new Business Opportunities, Mar. 2017. Available at: https://5g-ppp.eu/roadmaps/

[7] 5G Infrastructure Association (5G-IA), "5G Pan-European Trials Roadmap Version 4.0," November 2018. Available at: https://5g-ppp.eu/5g-trials-roadmap/

[8] European 5G Observatory, https://5gobservatory.eu

[9] F. Bastia et al., "LTE Adaptation for Mobile Broadband Satellite Networks," EURASIP J. on Wir. Commun. and Net., Nov. 2009.

[10] G. Araniti et al., "Efficient Resource Allocation for Multicast Transmissions in Satellite-LTE Network," in IEEE Glob. Comm. Conf. (GLOBECOM), pp. 3023-3028, Atlanta (US), Dec. 2013.

[11] M. Amadeo et al. "A Satellite-LTE network with delay-tolerant capabilities: design and performance evaluation," in IEEE Vehic. Tech. Conf. (VTC Fall), pp. 1-5, San Francisco (US), Sep. 2011.

[12] A. Guidotti et al., "Satellite-Enabled LTE Systems in LEO Constellations," in IEEE ICC Int. Work. on Sat. Commun. - Chall. and Integr. in the 5G ecosystem, pp. 876-881, Paris (FR), May 2017.

[13] A. Guidotti et al., "LTE-based Satellite Communications in LEO Mega-Constellations," IJSCN Sp. I. on SatNEx IV, pp. 1-15, Jun. 2018.

[14] 3GPP R1-171450, "Study on NR to support Non-Terrestrial Networks," 3GPP TSG#76, Jun. 2017.

[15] 3GPP TR 38.821, "Solutions for NR to support non-terrestrial networks (NTN) (Release 16)," June 2019.

[16] 3GPP TR 38.811, "Study on New Radio (NR) to support non terrestrial networks (Release 15)," June 2019.

[17] O. Kodheli, et al., "Integration of Satellites in 5G through LEO Constellations," IEEE Glob. Comm. Conf. (GLOBE- COM), pp. 1-6, Singapore, Dec. 2017.

[18] A. Guidotti et al., "Integration of 5G Technologies in LEO Mega-Constellations," IEEE 5G Tech Focus, Mar. 2018. Available at: https://arxiv.org/abs/1709.05807

[19] A. Guidotti et al., "Architectures and Key Technical Challenges for 5G Systems Incorporating Satellites," *IEEE Trans. on Veh. Tech.*, vol. 68, no. 3, Mar. 2019.

[20] A. Guidotti, "Beam Size Design for New Radio Satellite Communications Systems," *accepted for publication on Trans. on Veh. Tech. letters*, Sep. 2019.

[21] H2020-ICT-2014-1 Project VITAL, Deliverable D2.3, "System Architecture: Final Report," June 2016.

[22] H2020-ICT-2014-1 Project SANSA, Deliverable D2.3, "Definition of reference scenarios, overall system architectures, research challenges, requirements and KPIs," January 2016. Available at: http://www.sansa-h2020.eu/deliverables

[23] Robert M. O'Donnel, "Radar System Engineering - Lecture 9: Antennas," Radar System Course, IEEE New Hampshire Section, January 2010.

[24] ITU-R Recommendation P.676-11, "Attenuation by atmospheric gases," September 2016.

[25] ITU-R Recommendation P.618-13, "Propagation data and prediction methods required for the design of Earth-space telecommunication systems," December 2017.

[26] ITU-R Recommendation P.531-13, "Ionospheric propagation data and prediction methods required for the design of satellite services and systems," September 2016.

[27] 3GPP TR 36.829, "Enhanced performance requirement for LTE User Equipment (UE) (Release 11)," January 2013.